# UC Berkeley

## UC Berkeley Previously Published Works


### Title

The clumped-isotope geochemistry of exhumed marbles from Naxos, Greece


### Permalink

https://escholarship.org/uc/item/5g57x3ff



### Authors

Ryb, U
Lloyd, MK
Stolper, DA
et al.



### Publication Date

2017-07-01

### DOI

10.1016/j.epsl.2017.04.026

Peer reviewed



eScholarship.org Powered by the California Digital Library
University of California

# The clumped-isotope geochemistry of exhumed marbles from Naxos, Greece

U. Ryb, M.K. Lloyd, D.A. Stolper, J.M. Eiler

Abstract

Exhumation and accompanying retrograde metamorphism alter the compositions and textures of metamorphic rocks through deformation, mineral–mineral reactions, water–rock reactions, and diffusion-controlled intra- and inter-mineral atomic mobility. Here, we demonstrate that these processes are recorded in the clumped- and single-isotope (δ13Cand δ18O) compositions of marbles, which can be used to constrain retrograde metamorphic histories.

We collected 27 calcite and dolomite marbles along a transect from the rim to the center of the metamorphic core-complex of Naxos (Greece), and analyzed their carbonate single- and clumped-isotope compositions. The majority of Δ47 values of whole-rock samples are consistent with exhumation- controlled cooling of the metamorphic complex. However, the data also reveal that water–rock interaction, deformation driven recrystallization and thermal shock associated with hydrothermal alteration may considerably impact the overall distribution of Δ47 values.

We analyzed specific carbonate fabrics influenced by deformation and fluid–rock reaction to study how these processes register in the carbonate clumped-isotope system. Δ47 values of domains drilled from a calcite marble show a bimodal distribution. Low Δ47 values correspond to an apparent temperature of 260 °C and are common in static fabrics; high Δ47values correspond to an apparent temperature of 200 °C and are common in dynamically recrystallized fabrics. We suggest that the low Δ47 values reflect diffusion-controlled isotopic reordering during cooling, whereas high Δ47 values reflect isotopic reordering driven by dynamic recrystallization. We further studied the mechanism by which dynamic recrystallization may alter Δ47 values by controlled heating experiments. Results show no significant difference between laboratory reactions rates in the static and dynamic fabrics, consistent with a mineral-extrinsic mechanism, in which slip along crystal planes was associated with atomic-scale isotopic reordering in the calcite lattice. An intrinsic mechanism (enhanced isotopic reordering rate in deformed minerals) is contraindicated by these experiments. We suggest that Δ47 values of dynamically recrystallized fabrics that form below the diffusion-controlled blocking-temperature for calcite constrain the temperature of deformation.

We find that Δ47-based temperatures of static fabrics from Naxos marbles are ~60–80 °C higher than commonly observed in slowly cooled metamorphic rocks, and would suggest cooling rates of ~105°CMyr−1. A similar thermal history is inferred for dolomite marbles from the core vicinity, which preserve apparent temperatures up to 200 °C higher than a typical

blocking temperature (~300 °C). This finding could be explained by a hydrothermal event driving a brief thermal pulse and locally resetting Δ47 values. Rapid cooling of the core-complex region is consistent with a compilation of published cooling ages and a new apatite U–Th/He age, associating the thermal event with the emplacement of a granodioritepluton at ~12 Ma.

Keywords: clumped isotopes, retrograde metamorphism, dynamic re-crystallization, thermal history, exhumation, core-complex

## 1. Introduction

Metamorphism alters the compositions and textures of rocks through both physical deformation and chemical reactions, in both open and closed systems (i.e., with respect to fluids or melts). Metamorphic fabrics result from both prograde processes and over-printing retrograde processes (Shelley, 1993). Understanding these processes in a quantitative manner is needed to reconstruct the temperature, pressure, deformation/stress, and compositional histories of metamorphic rocks.

Metamorphic histories are often reconstructed using mineral assemblages (e.g. Jansen and Schuiling, 1976), elemental and isotopic compositions of various phases (e.g. Essene, 1989), and structural analyses of deformed (dynamic) and undeformed (static) fabrics (e.g. Burkhard, 1993). Here, we explore how different retrograde processes are recorded by the ‘clumped’ and carbon and oxygen isotopic compositions of marbles from Naxos, Greece. We demonstrate the potential of clumped-isotope thermometry to quantitatively constrain the chemical, thermal, and deformational histories of rocks during retrograde metamorphism.

### 1.1. Carbonate clumped-isotope thermometry of exhuming marbles

Carbonate clumped-isotope thermometry is based on the preferential bonding of C13 to O18in the same carbonate group relative to a random distribution of isotopes amongst all carbonates. The degree of such isotopic ordering is reported using the Δ47 value, which is the relative difference, in per mil, between the measured abundance of mass 47 isotopologues (97% of which are C1813O16O, Ghosh et al., 2006) in $CO_2$ released during acid digestion of a carbonate bearing mineral vs. the abundance of mass 47 that would be observed if all isotopes were randomly distributed amongst all isotopologues (Wang et al., 2004). In carbonate minerals that are in internal isotopic equilibrium, Δ47 values are a small positive number (‰~0.5‰) and decline with increasing temperature (Ghosh et al., 2006). Calcite, dolomite aragonite, and carbonate groups in apatite have been shown to share the same Δ47-temperature equilibrium calibration (Bonifacie et al., 2017, Stolper and Eiler, 2015).

Clumped-isotope thermometry is commonly used to constrain the formation temperatures of carbonate minerals from Earth-surface environments (Eiler, 2011). At temperatures >100 °C Δ47 values may alter through solid-state

reordering (Passey and Henkes, 2012). In such cases, initial Δ47 values that reflect Earth-surface temperature may decrease and approach values characteristic of higher temperature crustal environments. The rate of such changes is controlled by the kinetics of solid-state reordering of C–O bonds. Given sufficiently high temperatures and long times (as often occurs in metamorphic environments), buried sedimentary carbonates may fully re-equilibrate Δ47 values to their new temperatures. Cooling from high temperature, Δ47 values are expected to follow thermodynamic equilibrium until temperature becomes too low to permit isotopic reordering, at which point the Δ47 value is locked in (Fig. 1A). Stolper and Eiler (2015) have called this lock-in temperature the ‘apparent equilibrium blocking temperature’, and used ‘apparent temperatures’ when measured temperatures did not refer to any specific process. Here, we follow the above definitions, but use ‘blocking temperatures’ and ‘apparent temperatures’ for simplicity. The blocking temperature is a function of the cooling rate (Fig. 2).

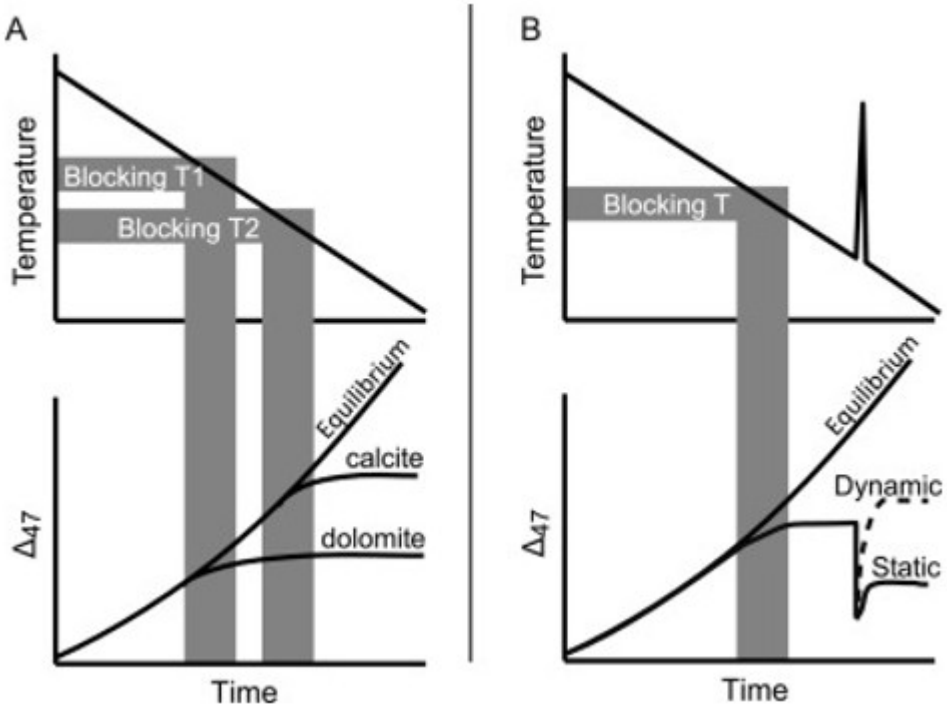


Fig. 1. Conceptual diagrams depicting various example thermal and deformational histories and the expected changes in $\Delta_{47}$ values due to solid-state isotopic reordering. A) Linear cooling scenario; T1 and T2 mark the range of temperatures in which calcite and dolomite cease changing in $\Delta_{47}$ due to a decrease in the rate of internal isotope-exchange processes. Based on previous observations (Bonifacie et al., 2013, Ferry et al., 2011, Ghosh et al., 2006) calcite continues to exchange isotopes internally at lower temperatures than dolomite. This leading to a higher final observed $\Delta_{47}$ value in calcite relative to dolomite given the same thermal history. B) A more complicated thermal/deformational history. Such a history could explain the results of sample NAX2, which are presented and discussed in details in sections 3.1–3.3. After the calcite had cooled below its $\Delta_{47}$-based blocking temperature, it sustains a brief heating event. This is followed by local shear deformation in some fabric and leading to two final observed $\Delta_{47}$ values for the static and dynamically recrystallized fabrics.

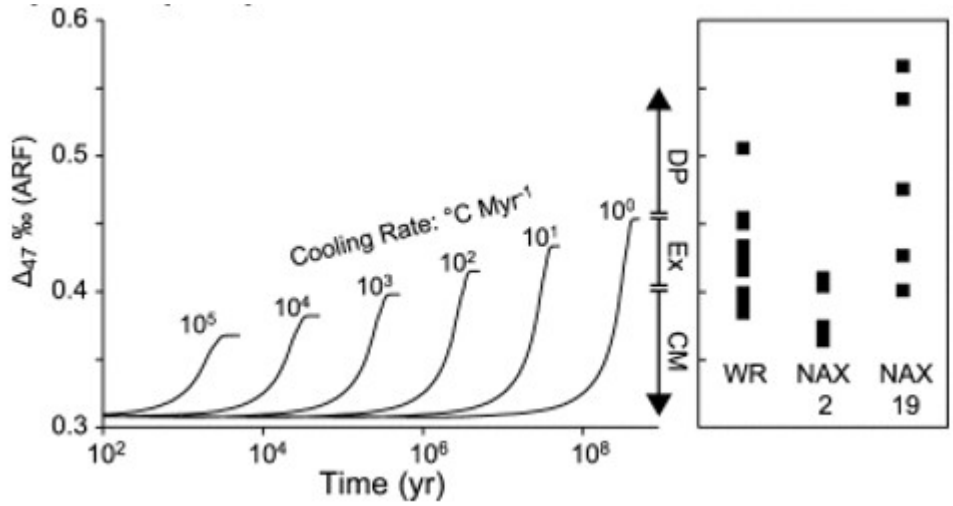


Fig. 2. Time evolution of $\Delta_{47}$ values for calcite experiencing different cooling rates. $\Delta_{47}$ values were calculated using the 'reaction–diffusion' model of Stolper and Eiler (2015) for a series of thermal histories in which temperature decrease from 500 °C at different rates. Final observed $\Delta_{47}$ values decrease with increasing cooling rate. Providing that the initial temperature is above the blocking temperature of calcite, it has a negligible effect over the final-observed $\Delta_{47}$ (Fig. DR1). Based on the cooling rates, the range of $\Delta_{47}$ values is divided between contact metamorphism (CM) and exhumation (Ex), for cooling rates above and below 1000 °C $Myr^{-1}$, respectively. Higher $\Delta_{47}$ values (reflecting colder apparent temperatures) cannot be explained by cooling from high temperature, and require recrystallization below the blocking temperatures of calcite through dissolution–precipitation (DP) or other process. The ranges of $\Delta_{47}$ values of calcite marbles whole-rock (WR), and subsamples of two calcite marbles (NAX2 and NAX19), are wider than the expected range of values for a simple exhumation controlled cooling scenario.

Δ47-based apparent temperatures of calcite marbles show a range of ~150–200 °C, which can be explained by geologically plausible, exhumation-controlled cooling rates (1–1000 °C $Myr^{-1}$) (Passey and Henkes, 2012, Stolper and Eiler, 2015). Higher apparent temperatures in exhumed carbonate-bearing metamorphic rocks would require faster cooling rates, as might occur in some hydrothermal and contact-metamorphism environments (Bristow et al., 2011, Passey and Henkes, 2012, Stolper and Eiler, 2015). It has been found that isotopic reordering in dolomite is more refractory to changes during slow cooling as compared to calcite, suggesting blocking temperatures for geologically common thermal histories of ~300 °C for dolomite vs. 150–200 °C for calcite (Bonifacie et al., 2013, Ferry et al., 2011, Ghosh et al., 2006, Lloyd et al., 2017).

Previous studies have measured carbonate clumped-isotope compositions of only a limited number of calcite marble samples, the majority of which are Carrara Marbles that are commonly used as an inter-laboratory standard (e.g. NBS19). These samples are analyzed as aliquots of powdered whole-rocks. Such homogenization could obscure hand-sample scale heterogeneity that may arises from localized heating, or recrystallization following dissolution–precipitation or deformation (Siman-Tov et al., 2016, Swanson et al., 2012). Deformation may affect mineral composition by facilitating reaction kinetics and local temperature gradients via shear-heating (Rutter and Brodie, 1995). For example, Siman-Tov et al. (2016),

suggested that the formation of nano-size calcite-grains along faulting planes accelerates isotopic reordering during and after the faulting of carbonate rocks.

Here, we analyze calcite and dolomite marbles across the metamorphic core-complex of Naxos (Greece), and explore how different retrograde metamorphic processes are recorded by their single- and clumped-isotope compositions. We focus our examination on variations in clumped-isotope composition of calcitic and dolomitic fabrics that appear to result from water–rock reactions and/or deformation.

### 1.2. Study area

Metamorphism of the Cycladic-Attic massif followed the Cenozoic convergence of Africa and Eurasia along the Hellenic subduction Zone (Ring et al., 2010) (Fig. 3A). During the Eocene, underthrusting of continental fragments at the accretionary prism resulted in a blueschist-facies metamorphism (M1) (Altherr et al., 1979, Andriessen et al., 1979, Schliestedt et al., 1987, Urai et al., 1990). Starting in the early Miocene, southward roll-back of the Hellenic Subduction Zone led to the opening of the Aegean back-arc basin, magmatism, and rapid exhumation of the underlying metamorphic complex. This overprinted the massif with a second metamorphic event at greenschist- to amphibolite-facies conditions (M2) (Altherr et al., 1979, Andriessen et al., 1979). Extension in the Aegean back-arc also resulted in the exhumation of the Hercynian basement and meta-sediments (Fig. 3B, ‘lower tectonic unit’) along low-angle detachment faults. This juxtaposed the Hercynian basement and meta-sediments against unaltered, or weakly metamorphosed Tertiary strata, (Fig. 3B, ‘upper tectonic unit’).

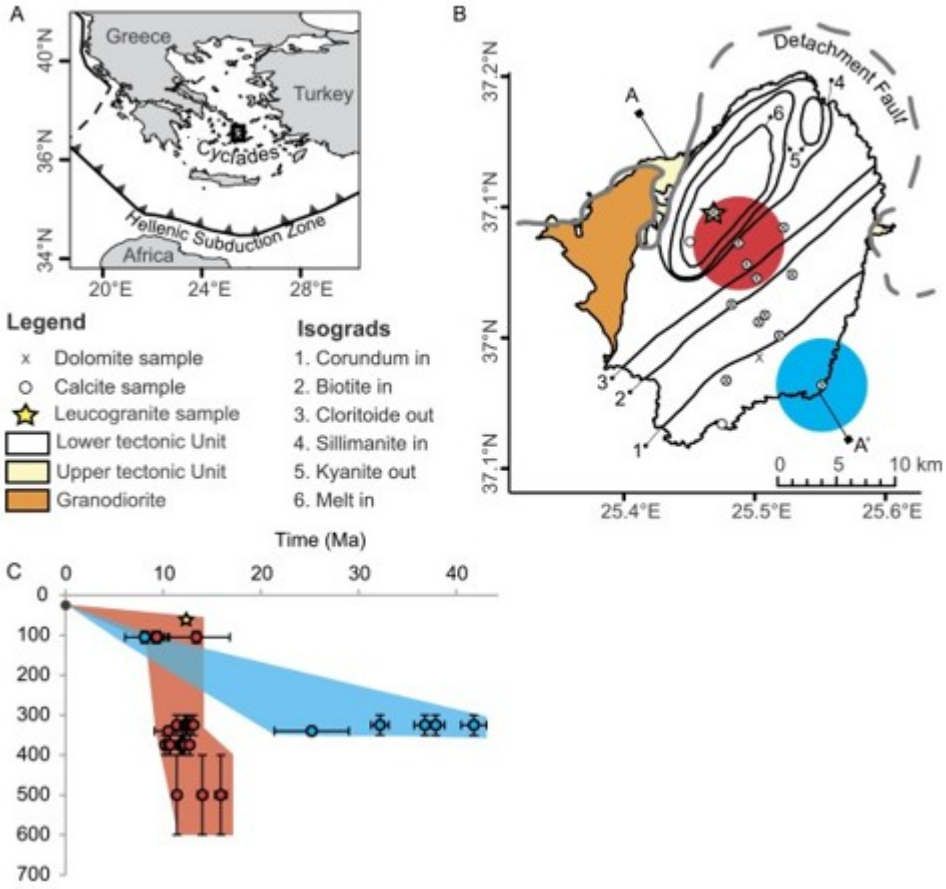


Fig. 3. A) Location map of the Aegean Sea and the Cyclades Islands, black rectangle delineates the location of Naxos. B) Map of Naxos metamorphic core-complex; geological contacts are based on Jansen and Schuiling (1976). Dashed gray line indicates the presumed location of the Naxos Detachment Fault. Red and blue circles mark the spatial extents of cooling-age compilations in insets C. C) Compilation of thermochronometry data within a distance <3 km from NAX2 sampling site, next to the core of the metamorphic complex (red dots, which define a range of time–temperature paths marked by a red polygon), and from NAX38 sampling site, at the southeastern rim of the metamorphic complex (blue dots, which define a range of time–temperature-paths marked by a blue polygon). Data was compiled from: Andriessen et al. (1979), Wijbrans and Mcdougall (1988), Seward et al. (2009), Hejl et al. (2003), and this study (yellow star symbol). Horizontal error bars in C are 2$\sigma$. Vertical error bars in C are the range of closure temperatures of different thermochronometers (Reiners et al., 2005).

As in other Cycladic islands, the lower tectonic unit on Naxos is a metamorphic core-complex (Fig. 3B; Jansen and Schuiling, 1976). This unit occupies most of the island area and consists of Hercynian basement and meta-sediments (schist and marble), increasing in metamorphic grade from the rim to the core of the complex (Jansen and Schuiling, 1976). At the core of the metamorphic complex, peak temperatures reached ~700 °C and partial melting occurred during the M2 event (Jansen and Schuiling, 1976). At the southeastern rim of the complex, peak temperatures remained below 400 °C, as indicated by the preservation of blueschist assemblages and Eocene Ar–Ar ages for micas (Avigad, 1998). At ~12 Ma the complex was intruded by a granodiorite pluton (Andriessen et al., 1979, Wijbrans and

Mcdougall, 1988), which now outcrops along the western coast of the island (Fig. 3B).

The thermal history of Naxos has been constrained using various thermochronometers, including hornblende, white-mica and biotite K–Ar and Ar–Ar (Andriessen et al., 1979, Wijbrans and Mcdougall, 1988), zircon and apatite fission-tracks (Brichau et al., 2006, Hejl et al., 2003, Seward et al., 2009) and U–Th/He (Brichau et al., 2006) dating. These data suggest that the core of the metamorphic complex underwent rapid cooling during the mid-Miocene (Fig. 3C). We will consider multiple possible causes for this cooling history, but previous studies have attributed it to the tectonic exhumation of the lower tectonic unit (Brichau et al., 2006, John and Howard, 1995, Seward et al., 2009). At the southeastern rim of the complex, Ar–Ar ages are widely scattered (20–45 Ma), suggesting that M1 ages were only partially reset during the M2 event (Fig. 3D) (Andriessen et al., 1979, Seward et al., 2009, Wijbrans and Mcdougall, 1988).

Several generations of mineralization have been recognized in Naxos (Baker et al., 1989; Baker and Matthews, 1994, Baker and Matthews, 1995; Rye et al., 1976, Siebenaller et al., 2013) and in other islands across the Cyclades (Ganor et al., 1994). In Naxos, $\delta^{18}O$ and $\delta^{13}C$ compositions of secondary carbonate minerals and quartz decrease from the rim to the core of the metamorphic complex (Baker and Matthews, 1995, Matthews et al., 2002, Rye et al., 1976). Previous studies have attributed this trend to isotopically depleted fluid sources, resulting from the dehydration of pelite units during prograde metamorphism (Baker et al., 1989, Bickle and Baker, 1990), exsolution of fluid from anatectic melts during the peak temperature of the M2 event (Baker and Matthews, 1995, Matthews et al., 2002, Siebenaller et al., 2013), and/or hydrothermal circulation of meteoric water following mid Miocene magmatic activity (Baker and Matthews, 1995).

## 2. Methods

We collected 14 calcite marbles and 13 dolomite marbles from the lower tectonic unit of the Naxos core-complex. Sampling roughly followed a NW–SE transect from the core to the rim of the complex (Fig. 3B, detailed sampling map and description of key sampling sites are given in data repository item DR2). In one site we also collected a leucogranite sample for apatite U–Th/He dating (NAX37). Although some samples are texturally homogeneous, others display a range of metamorphic fabrics, including color bands, mylonite, and apparent post-M2 mineralization.

Whole-rock splits of marble samples were washed clean, dried, crushed and sieved to <106 μm fraction. The proportions of calcite and dolomite were determined using a 2D Phaser Bruker XRD system at Caltech. Single- and clumped-isotope measurements of carbonate whole-rocks were analyzed by phosphoric acid digestion and gas source mass spectrometry of evolved $CO_2$. Samples that consist of ≥98% calcite or dolomite were treated as one or the other phase, and dissolved at 90 °C. Otherwise, calcite and dolomite

components of mixed samples were separated by stepped acid digestion at 25 °C for calcite and 50 °C for dolomite, following the procedures described in Lloyd et al. (2017). Extracted $CO_2$ from all samples and standards was purified cryogenically and on a GC column and analyzed over multiple sessions during replication using a MAT 253 mass spectrometer (Thermo) at Caltech. Measurements were standardized to heated and water-equilibrated gases and in-house carbonate standards following procedures described by Ghosh et al. (2006), Huntington et al. (2009), and Passey et al. (2010), and are reported in the absolute reference frame (Dennis et al., 2011). Δ47 values were corrected for acid fractionation at different temperatures of digestion following Defliese et al. (2015). We calculated apparent temperatures based on Stolper and Eiler's (2015)Δ47-temperature calibration. Oxygen and carbon single-isotope measurements are reported relative to VSMOW and VPDB standards.

In addition to measurements of whole-rock samples, we conducted detailed studies of individual components of three marble samples that contained deformation fabrics (NAX2 and NAX19) and/or dissolution and precipitation fabrics (NAX9 and NAX19). These samples were cut in half, perpendicular to the orientation of the dominant layered fabrics. One half was thin sectioned and the other sampled with a micro-drill for single- and clumped-isotope measurements as described above. Major and minor element abundances of differing domains in the thin-sectioned half of each sample were analyzed using the Energy Dispersive Spectroscopy (EDS) system of the Zeiss 1550VP housed at Caltech to characterize and distinguish between different mineral components. In one sample (NAX19), we used the Electron Back-Scatter Diffraction (EBSD) system of the Zeiss 1550VP to map preferred crystal orientation.

In order to characterize the isotopic reordering kinetics of static and dynamic fabrics of sample NAX2, we performed controlled heating experiments on large (3–4 mm) fragments broken from each fabric. These fragments were sealed in quartz-glass tubes with ~0.1 atm $CO_2$ enriched in δ18O (47.4‰) and depleted in δ13C (‰−11‰) relative to the marble. The tubes were then heated to 536 °C for 0.5, 1, and 1.5 h intervals. This temperature was chosen to match a temperature used in the experiments of Stolper and Eiler (2015). To obtain samples large enough for clumped-isotope analysis, we combined, crushed and mixed 2–4 fragments from each experiment (all of which were subjected to the same time–temperature history). This formed a total of six separate replicate samples for each fabric (static or dynamic) in every time-interval. Single- and clumped-isotope compositions were measured following the methods described above.

Apatite grains were extracted from sample NAX37 (leucogranite). We selected five apatite grains using a binocular microscope, based on their size, morphology, and lack of inclusions. He, U and Th were analyzed using a quadrupole mass spectrometer (He) and a Thermo Scientific Element

inductive coupled plasma mass-spectrometer (U and Th), following the procedures described in the data repository of Flowers et al. (2008).

## 3. Results and discussion

A table of single and clumped-isotope compositions is presented in data repository item DR3. Our data for whole-rock samples of dolomite and calcite generally have δ18O and δ13Cvalues that overlap with published ranges for calcite and dolomite marbles from Naxos and other Cycladic islands (hereafter ‘primary range’) (Baker and Matthews, 1995) (Fig. 4). Several dolomite and calcite samples fall outside of the primary range toward lower δ18Oand δ13C values.

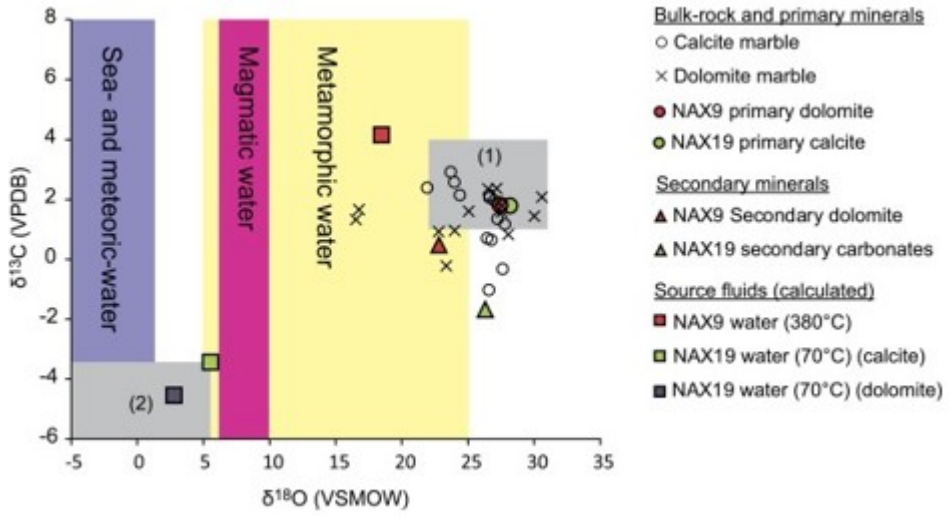


Fig. 4. $\delta^{18}O$ and $\delta^{13}C$ compositions of whole-rock calcite and dolomite marbles, secondary carbonates, and calculated source fluids. Grey rectangles mark: (1) the ‘primary range’ composition of Naxos marbles (Baker and Matthews, 1995), and (2) the calculated range of fluid in equilibrium with NAX19 secondary carbonates (see text for details). Color rectangles mark $\delta^{18}O$ ranges of different water sources (Taylor, 1974). Error bars (1 S.D.) are smaller than the size of the symbols.

Whole-rock Δ47 values for calcite range ‰0.384–0.505‰ and are systematically higher (i.e., implying lower apparent temperatures) than those for dolomite (‰0.306–0.379‰). This difference is consistent with calcite's faster inferred rate of isotopic reordering (Fig. 1A) (Bonifacie et al., 2017, Lloyd et al., 2015). Across the core-complex, the whole-rock apparent temperatures of calcite marbles do not show any obvious spatial trend (Fig. 5A, B). Toward the rim of the core-complex, whole-rock apparent temperatures of dolomite marbles are 328±53°C, and thus similar to typical blocking temperatures (~300 °C). Near the center of the core-complex, apparent temperatures are 413±61°C, and thus significantly higher than typical blocking temperatures. Within the area defined by the higher apparent temperature of dolomite marbles, calcite and dolomite grains become coarser towards the northwest (Fig. 5C).

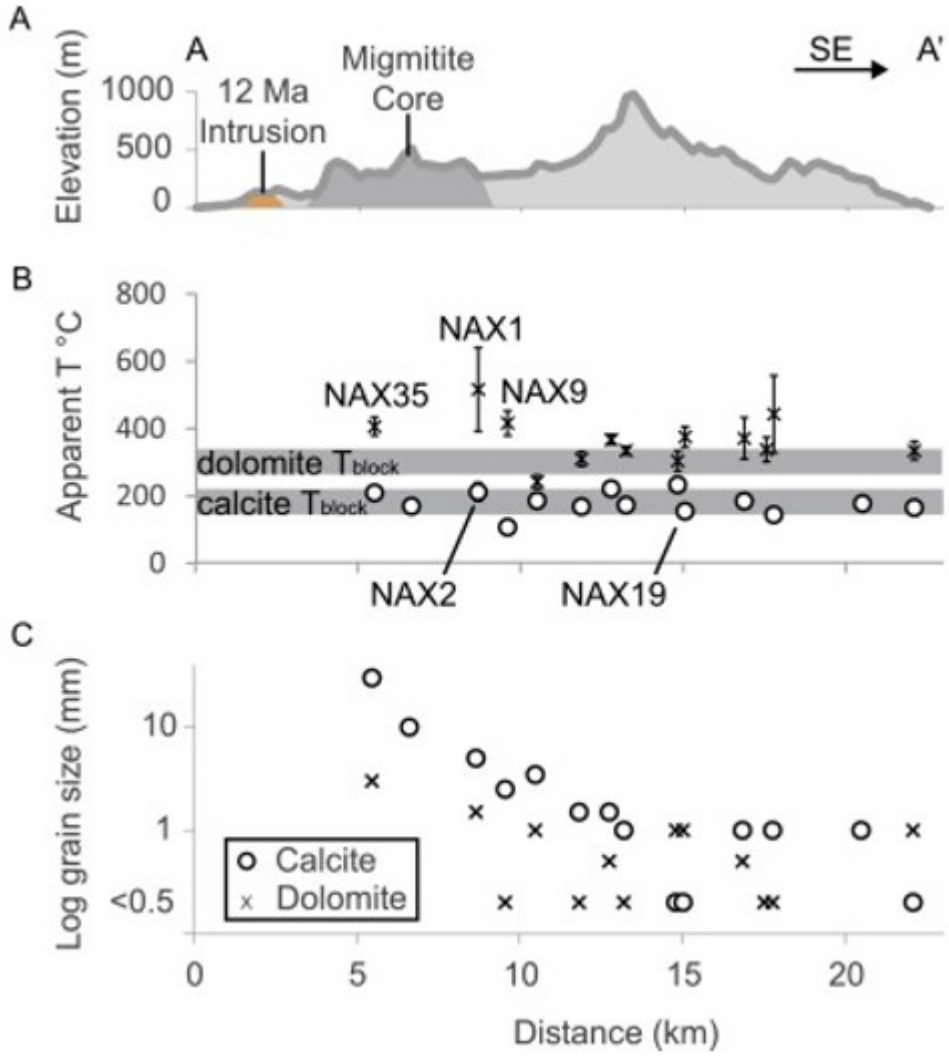


Fig. 5. A) A simplified geological NW–SE transect across Naxos metamorphic core-complex (see Fig. 3B for location). B) $\Delta_{47}$ based apparent temperatures of calcite (circles) and dolomite ('x' symbols) whole-rock marbles. Values from all sampling sites were projected onto the transect. Grey rectangles mark the expected ranges of exhumation controlled blocking temperatures for calcite (150–200 °C) and dolomite (270–330 °C). Error bars are 1 S.E., or if not present, smaller than the size of the symbol. C) Calcite and dolomite marbles dominant grain size, measured with a ruler. Values from different sites were projected onto the transect. In the inner 5 km of the core-complex, grains become coarser toward the northwest.

The Δ47 values for whole-rock calcitic marbles can be compared to those values expected based on the experimentally-constrained kinetics of solid-state isotopic reordering (Stolper and Eiler, 2015): Assuming a range of exhumation-controlled cooling rates of 1–1000 °C $Myr^{-1}$, one would expect Δ47 values for calcite of ‰0.41–0.45‰ – a considerably narrower distribution than we observe (Fig. 2). While the majority of whole-rock calcite marbles are within the expected range of Δ47 values, some Δ47 values are inconsistent with any plausible, exhumation-controlled cooling of the core-complex. There are currently no published rate constants that describe the kinetics of solid-state isotope reordering for dolomites that can be used for a

similar exercise, however, Δ47 values measurements of dolomite marbles that have experienced a range of cooling rates up to 104°CMyr−1, are typically ‰0.34–0.36‰ (Bonifacie et al., 2013, Ferry et al., 2011, Lloyd et al., 2017). The Δ47values we observe for dolomitic marbles overlap the expected value, but are, on average, lower than would be predicted using a simple cooling history.

These findings imply that some Δ47 values of Naxos marbles were influenced by processes other than a solid-state isotopic reordering during exhumation-controlled cooling. These rocks may have been influenced by a more complex temperature–time histories (e.g., brief and/or local high temperature events); some effect of deformation on solid-state isotopic reordering; and recrystallization and/or water–rock reaction. It is noteworthy that the standard deviation of whole-rock Δ47 values was frequently greater than that of individual measurements of our in-house Carrara marble measured during the same sessions (‰±0.016‰; table DR3), suggesting a hand-sample-scale heterogeneity of Δ47 values. We continue exploring the causes of variability of Δ47 values by sampling and analyzing specific fabrics at scales smaller than hand samples.

3.1. Deformation as a direct and indirect cause of Δ47 variations

Sample NAX2 is a calcite marble that was collected near the core of the metamorphic complex (Fig. 5B). It consists of alternating, 1–2 cm thick, white and gray color bands (Fig. 6A). Thin-section examination reveals that white and gray bands differ in grain size and texture: In the white bands, grains are large (1–5 mm) and have straight grain boundariesand well developed triple junctions, indicative of a static recrystallization process (Fig. 6B, also note the grain-boundaries on the SEM image in the online data repository item DR4). In the gray bands, we observe smaller grains (0.2–2 mm), serrated grain boundaries and twin lamella, and sub-grain rotation; all indicative of a dynamic recrystallization process (Fig. 6C) (Shelley, 1993). At the boundary between white and gray bands we observe unduluse extinction and sub-grain rotation at the edges of large crystals, indicating that dynamic recrystallization followed static recrystallization (Fig. 6D). We conclude that the rock experienced shear deformation that was localized in gray bands but left white bands mostly undeformed.

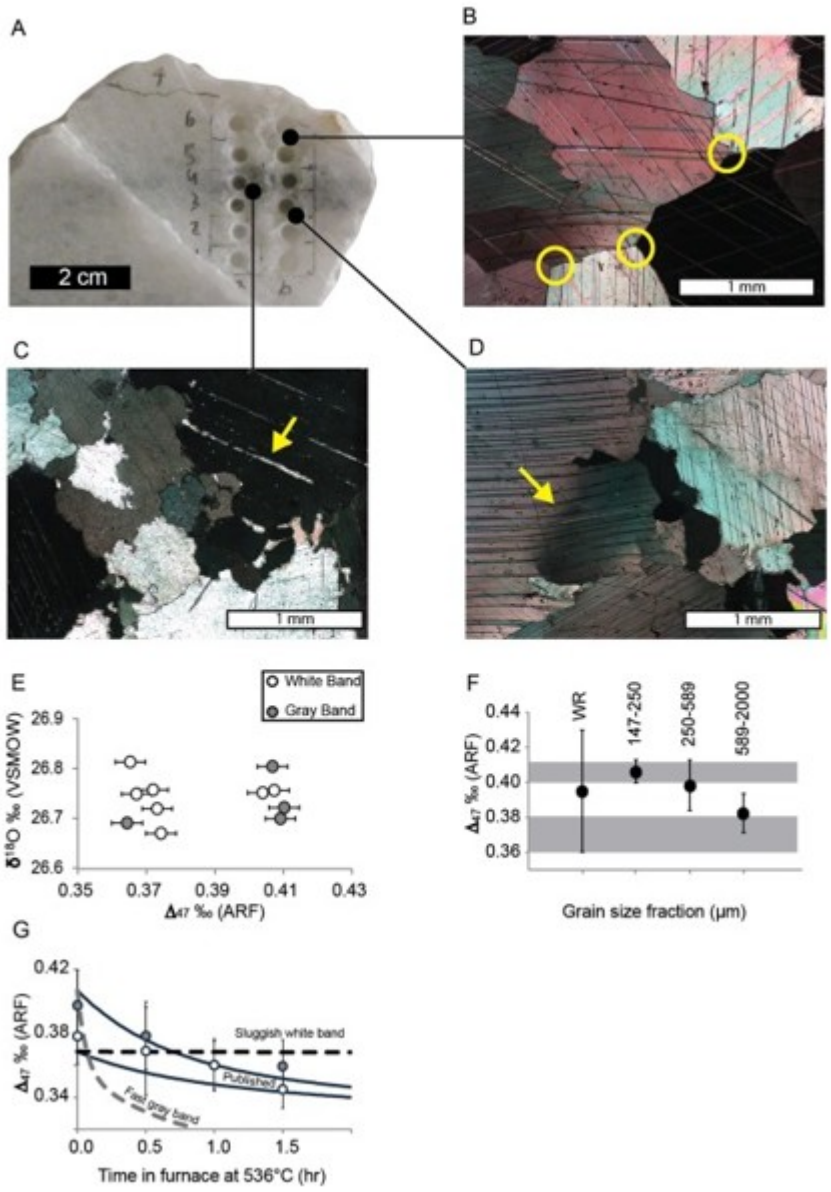


Fig. 6. Thin-section and carbonate clumped- and single-isotope analyses results of sample NAX2. A) Photograph of sample NAX2 showing white and gray color bands and drill-holes from which sub-samples were extracted. B) Thin-section image (crossed nicols) of a white band. Plain grain boundaries and triple-junctions (yellow circles) are indicative of static recrystallization (Shelley, 1993). C) Thin-section image (crossed nicols) of a gray band. Serrated grain boundaries and twin-lamellas (yellow arrow) are indicative of dynamic recrystallization (Shelley, 1993). D) Thin-section image (crossed nicols) of a contact between white and gray bands, unduluse extinction at the grain margin (yellow arrow), is indicative of sub-grain rotation during dynamic recrystallization (Shelley, 1993). E) $\Delta_{47}$ values of subsamples from white and gray color bands, plotted against the samples $\delta^{18}O$ values. F) $\Delta_{47}$ values of different grain-size fraction of sample NAX2; gray rectangles mark the high and low modes of $\Delta_{47}$ values observed in drilled subsamples (panel E). WR is whole-rock value, based on the <147 μm grain-size fraction. G) Controlled heating experiment results for white and gray calcite fragments. Lines are the predicted reaction progress trends calculated with Stolper and Eiler (2015) 'reaction–diffusion' model. Solid black lines (labeled 'Published') are based on the initial $\Delta_{47}$ values of the two modes in panel 'E', and using the published rate constants. Dashed gray line ('Fast gray band') is based on initial $\Delta_{47}$ values of the higher mode in panel 'E', and an order of magnitude higher reaction rates. Dashed black line ('Sluggish white band') is based on initial $\Delta_{47}$ values

of the lower mode in panel ‘E’, and an 3–4 orders of magnitude lower reaction rates (see text for details). Predicted $\Delta_{47}$ values were converted to the Absolute reference frame (ARF) from Caltech's reference frame (CRF) using: $\Delta_{47(ARF)} = 1.064\Delta_{47(CRF)} + 0.026$; This relation was observed between $\Delta_{47}$ values that were calculated in both reference frames for our whole-rock sample and in-house standards (Data repository Item DR7). Error bars are 1 S.D.

Subsamples of white or gray bands share a common carbon and oxygen isotopecomposition, consistent with the ‘primary range’.
Conversely, Δ47 values have a clear bimodal distribution: High Δ47 values (‰0.404–0.410‰), corresponding to an apparent temperature of 200 °C are common in the gray bands; whereas low Δ47 values (‰0.364–0.374‰), corresponding to an apparent temperature of 260 °C are common in the white bands (Fig. 6E). Generally, white bands have lower Δ47 values while gray bands have higher Δ47 values. However, there are exceptions to this (Data repository Item DR5). This may reflect the imperfection of our identification of boundaries of color bands in the drilled slab, or that processes correlated but not always associated with color, control Δ47 values. The whole-rock Δ47 value of this sample (0.397±0.035, 1 S.D) overlaps within error both the high and low modes of Δ47 values observed in the drilled subsamples. We further studied the distribution of Δ47 values within the sample by analyzing multiple grain-size fractions of the crushed sample (Fig. 6F). The Δ47 values of the 147–250 μm and 589–2000 μm grain-size fractions (‰0.406±0.007‰ and ‰0.382±0.011‰) overlap the ranges of high and low Δ47 values observed in the drilled subsamples, respectively. This is consistent with our findings for drilled samples, because deformed fabrics consist of smaller and more friable grains and are therefore expected to dominate the smaller grain size fraction, whereas static fabrics consist of larger and less-friable grains and thus are expected to dominate the largest grain-size fraction (which largely consists of single-crystal grains). The results of the grain-size fraction analyses strengthen the association between the high or low modes of Δ47 values, with deformed (gray band) or static (white band) fabrics, respectively.

This mm-scale variation of Δ47 values could potentially reflect (1) some amount (10s of percent) of dolomite in the (mostly) white bands because dolomite is systematically lower in Δ47 than calcite; (2) localized thermal shock resulting from shear-heating of the (mostly) white bands; (3) localized precipitation of calcite at a higher or a lower temperature. Or, (4) a deformation driven change in Δ47 values.

This first option is ruled out by EDS scans across white and gray band, which demonstrate that both bands consist of low Mg calcite with traces of mica and pyrite, but without any dolomite (scans are available in the online data repository item DR4). We reject the second option given above because dynamic recrystallization of the sort indicated by the grain textures of this rock is a slow process that does not involve local shear-heating. The third option is argued against by the lack of isotopic or petrographic evidence for re-precipitation in either the white or gray bands (e.g., the preservation of static and dynamic recrystallization features). We therefore

proceed with the hypotheses that the difference in Δ47 values between white and gray bands is either a direct consequence of deformation (i.e., dynamic recrystallization changed the Δ47 value of gray bands), or an indirect consequence of deformation history (i.e., white bands and gray bands differ in their isotopic reordering kinetics). The following sections attempt to distinguish between these two possible mechanisms, and address the implications of the low Δ47 values of static fabrics for the thermal history of the Naxos core-complex.

### 3.2. In what ways can deformation affect isotopic reordering in a carbonate mineral?

Controlled heating experiments have demonstrated that the process of solid-state isotopic reordering during high temperature (>400 °C) heating displays a non-first-order kinetics characterized by an initial fast drop in Δ47 values, followed by a slower decrease (Passey and Henkes, 2012, Stolper and Eiler, 2015). Passey and Henkes (2012) attributed the first, fast stage of reordering to an initially high concentration of lattice defects that accelerate C–O bond reordering but are annealed away rapidly. The later, slower stage of reordering is then controlled by the intrinsic rate of atomic mobility in the absence of the now annealed defects. According to their model, it might be reasonable to expect the rate constants that describe isotope-exchange in the carbonate to vary among calcite samples that have different defect densities. In contrast, Stolper and Eiler (2015) consider solid-state reordering as the result of two separate processes: (1) Isotope-exchange reactions occurring between two neighboring carbonate species, which may form a clumped carbonate species or break a clumped species to form two neighboring singly-substituted carbonate species (or an isotopologue ‘pair’); and (2) short-range diffusion of carbonate species that move C and O isotopes in the lattice. This model attributes the initial rapid change in Δ47 to the isotope-exchange reaction, and suggested that the slower reaction that followed was rate-limited by short-range diffusion. Similar kinetic parameters could fit optical calcites and brachiopod calcites, indicating that this model may be applicable to calcites of differing origins.

Following these models, we suggest two mechanisms by which deformation of carbonate minerals might promote oxygen, carbon, or carbonate mobility across the calcite lattice: 1) An intrinsic mechanism by which deformation increases O and C diffusivities in the crystal lattice by increasing defect-density; and 2) an extrinsic mechanism, in which slip along crystal planes efficiently transports carbonate ion groups across the crystal lattice and accelerates isotopologue ‘pair’ formation and destruction. If the intrinsic mechanism is correct, isotopic reordering of dynamic fabrics during laboratory heating experiments is expected to be faster than that in static fabrics (at least until those defects anneal), because deformed fabrics have, by definition, higher defect-densities (e.g., Karato, 2008). However, if the

extrinsic mechanism is correct, enhanced mobility occurs only during active strain, and we should find no such difference today.

We tested these predictions by heating static and dynamically recrystallized fabrics of sample NAX2 (white and gray bands, respectively) and comparing rates of change to model predictions. Samples were exposed to 536 °C for intervals of 0.5, 1, and 1.5 h (see methods section for full details). For each time interval, average Δ47 values decrease from initial values (Fig. 6G). The time-evolution in Δ47 for these two fabrics are indistinguishable from each other, and both are consistent, within uncertainties, with the model and published temperature-dependence of rate constants from Stolper and Eiler (2015) (Fig. 6G). The rates of Δ47 change in our experiment are also consistent with those observed for heating of other calcites by Passey and Henkes (2012), and Henkes et al. (2014). Thus, our experiment shows that the two fabrics are indistinguishable in isotopic reordering kinetics to other studied calcites of different origins. These experimental results are consistent with the hypothesized extrinsic mechanism.

An issue is whether the relative small (‰0.03–0.04‰) change in Δ47 in the experiments is sufficient to yield meaningful differences in reaction rate between white and gray bands if the intrinsic mechanism hypothesis was correct. Using the model of Stolper and Eiler (2015), we considered two alternative temperature histories that might explain our data for sample NAX2, and adjusted the ‘reaction’ and ‘diffusion’ rate constants (multiplying both by a single constant factor) to match the observed values of the high and low Δ47 modes:

1) *The ‘Fast gray band’ scenario* – Assuming the rate constants of static fabrics follow the temperature dependence given for calcite by Stolper and Eiler (2015) (their equations 18–19), a cooling rate of 105°CMyr−1 is required to explain the observed Δ47 value (Fig. 2). Whatever the plausibility of this finding (a point we address below), given this cooling rate, the rate of reordering of the dynamically recrystallized fabrics must be an order of magnitude higher than the static fabric.

2) *The ‘Sluggish white band’ scenario* – Assuming rate constants follow the temperature dependence as above but for the gray bands, a cooling rate of 300 °C $Myr^{-1}$ is required to explain the observed Δ47 value (Fig. 2). With this cooling rate, rate-constants of the white bands should be 3–4 orders of magnitude lower then published values to explain their Δ47value.

Modifying the rate-constants according to the two scenarios, we predict the expected reaction progress for the heating experiment. The resulting curves for both scenarios differ significantly from the data (Fig. 6G). Therefore our experimental findings are inconsistent with an intrinsic mechanism driving the observed bi-modality in Δ47 values. We conclude that this difference is better explained by extrinsic effects on isotopic reordering during dynamic recrystallization.

Our results suggest that Δ47 values of dynamically recrystallized fabrics reflect the minimum temperature of deformation. For a given stress, slip along crystal planes (specifically, the *r*and *f* planes in calcite) becomes increasingly sensitive to temperature between 250–150 °C (DeBresser and Spiers, 1997, their Fig. 11). Thus, blocking temperatures of ~200 °C are plausible minimum temperature for dynamic recrystallization of calcite.

### 3.3. Hot white bands

Low Δ47 values observed in sample NAX2 average ‰0.369±0.004‰ (1 S.D.), and are associated with static fabrics of (mostly) white bands. This value is interpreted to reflect the blocking temperature of calcite, and requires a cooling rate on the order of 105°CMyr−1, down to below ~150 °C (where Δ47 values become stable in respect to diffusion-controlled solid-state isotopic reordering over geological timescales; Stolper and Eiler, 2015). Given the evidence presented above, we suggest that a plausible explanation is that the sample experienced a thermal shock, reaching at least the temperature implied by their Δ47 value, followed by very rapid cooling, at rates greatly exceeding those achievable through exhumation (Fig. 2). Supporting this interpretation, dolomite sample NAX1, collected immediately next to NAX2, registered the lowest Δ47 value across our entire dataset (‰0.306±0.021‰ (1 S.E.)), corresponding to an apparent temperature of 516±124°C.

A compilation of published cooling ages from samples collected within 3 km of the NAX2 sampling site shows an overlap of hornblende, biotite and white mica K–Ar ages and zirconand apatite fission-track ages between 9–13 Ma. These various thermochronometers have blocking temperatures that range from 500 to 105 °C (Fig. 3C). We expanded this range by measuring apatite U–Th/He single-grain ages of sample NAX37, collected at the center of the core, ~3 km away from NAX2. The U–Th/He system blocking temperatures range ~40–80 °C (Farley, 2002). This analysis yielded an average age of 12.0±0.3 Ma, which is within the range of the other thermochronometers ages with higher blocking temperatures (Fig. 3C). The single grain U/Th–He results are available in online data repository item DR6. The correspondence of ages of the thermochronometers with differing blocking temperatures requires a cooling rate >240 °C $Myr^{-1}$ from 325 °C to less than 60 °C. Such a cooling rate is consistent with the brief thermal pulse we suggest could explain the low Δ47 value of static fabrics in sample NAX2.

Taken together, we interpret the variation in Δ47 values in sample NAX2 as a record of complex thermal and deformational history (Fig. 1B): First gradual cooling occurred to below the intrinsic blocking temperature (likely ~150–200 °C, as for other common calcite marbles); Second the samples were heated up to at least 516±124°C (based on the apparent temperature of sample NAX1), followed by rapid cooling. Finally, localized dynamic recrystallization occurred in shear-bands. This dynamic recrystallization would have been nearly simultaneous with (and perhaps triggered by) the

rapid heating; if the ~200 °C temperatures recorded by the dynamic fabrics were sustained, the static fabrics would have been reordered to lower temperatures. The fact that high apparent clumped isotope temperatures are preserved indicates rapid cooling following the heating event.

A plausible heat-source for the thermal pulse was the emplacement of the granodioritepluton at ~12 Ma (Andriessen et al., 1979, Wijbrans and Mcdougall, 1988) (Fig. 3C). The grain-coarsening trend within the center of the core-complex is consistent with crystal growthin response to a heat supply from a source in northwestern quadrant of the field area (Fig. 5C) during peak M2 metamorphism (Covey-Crump and Rutter, 1989) or on a later retrograde stage (following the hypothesized heat pulse). The location where we sampled the core-complex is >4 km away from the intrusion. We can estimate the dimension of a heat-source consistent with such rapid temperature change by calculating the characteristic diffusive timescale ($\tau$): Assuming a temperature difference of 300–700 °C between the heat-source and its environment, and dividing it by the cooling rate of 105°CMyr−1 we find τ=3–7 kyr. From $\tau$ we can derive a characteristic length scale ($l$) by:

(1)τ=l2κ;

where $\kappa$ is the rock thermal diffusivity (typically 1–2.5×10−6 sec $m^{-2}$; Whittington et al., 2009). Using the above relation, we get l=300–750 m, suggesting a heat source that was closer to our sample and smaller than the pluton. Alternative heat sources could include a local magmatic intrusion or advection of heat from the pluton via hydrothermal activity. We prefer the hydrothermal hypothesis as no magmatic bodies were observed in the proximity of the sampling site or are apparent on a geological map (Jansen and Schuiling, 1976); and since mineral-veins associated with hydrothermal activity were reported in the island, and specifically in and around the pluton (Baker and Matthews, 1995).

We further investigate the effects of heat-pulse and mineralization on one of the low-Δ47dolomite marbles (NAX9, Fig. 5B) from the center of the complex and on a high-Δ47 calcite marble from the rim of the complex (NAX19, Fig. 5B).

### 3.4. Further effects of the hypothesized hydrothermal event: dissolution, precipitation and a thermal pulse

Sample NAX9 is a dolomite marble with a whole-rock Δ47 value ‰0.322±0.008‰ (1 S.E.), collected next to the center of the core-complex. The sample consists of white dolomite, hosting veins of yellow dolomite that partially fill dissolution fissures (Fig. 7A). The host-rockhas a ‘core and mantle’ texture, indicative of dynamic recrystallization (Shelley, 1993). These primary grains are <200 μm and have twin lamella (Fig. 7B). Secondary dolomite in veins consists of 1–2 mm unstrained rhombs, indicating precipitation occurred after deformation (Fig. 7C). Immediately

next to the contact with the secondary minerals, primary dolomite grains appear to have undergone static recrystallization (annealing) (Fig. 7C).

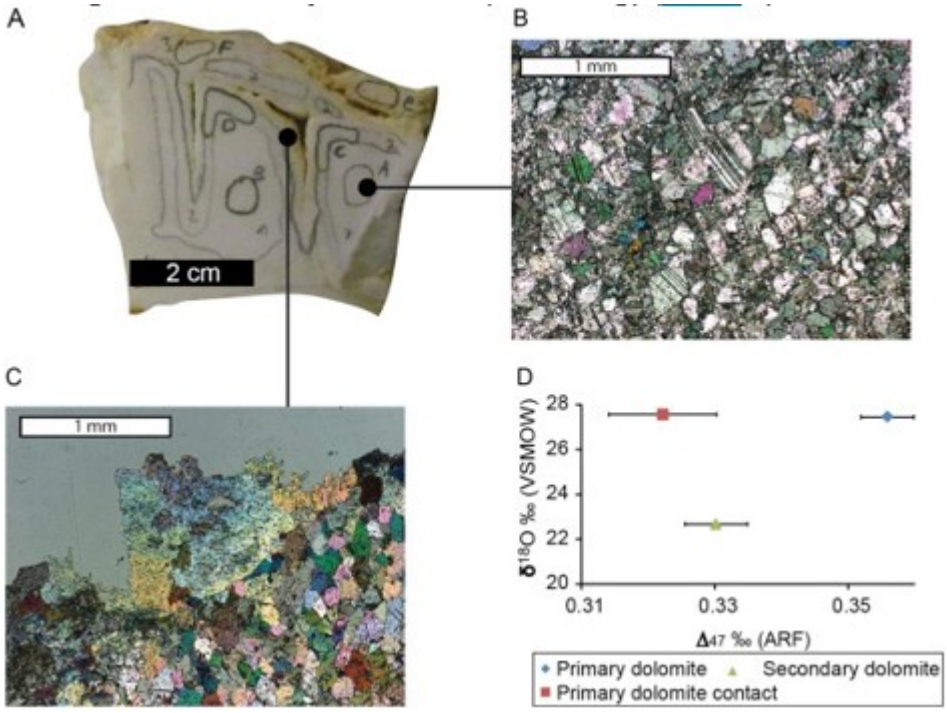


Fig. 7. Thin-section and carbonate clumped- and single-isotope analyses results of sample NAX9. A) Photograph of sample NAX9; the sample consists of white dolomite hosting veins of secondary yellow dolomite in dissolution fissures. Numbers refer to specific fabrics identified in the sample, and letters mark the specific locations from which subsamples were drilled (table DR3). B) Thin-section image (crossed nicols) of a primary dolomite. 'Core and mantle' structures are indicative of dynamic recrystallization(Shelley, 1993). Grain cores are typically twinned. C) Thin-section image (crossed nicols) showing large secondary dolomite rhombs. Close to the secondary minerals vein, primary dolomite grains were annealed. D) $\Delta_{47}$ values of dolomite subsamples plotted against $\delta^{18}O$ composition. Error bars are 1 S.E. for $\Delta_{47}$ values, and smaller than the symbol for $\delta^{18}O$.

Dolomite fabrics of sample NAX9 yield a range of single- and clumped-isotope values (Fig. 7D); primary dolomite has a Δ47 value of ‰0.356±0.004‰ (1 S.E.), corresponding to a blocking temperature of 290 °C, and δ18O and δ13C values of 27.4 and 1.8‰, respectively, consistent with the 'primary range'. Secondary, vein-filling dolomite has a significantly lower Δ47 value of ‰0.330±0.005‰ (1 S.E.), corresponding to an apparent temperature of 380 °C. This is above the previously observed blocking temperatures of 300–350 °C found for dolomites marbles from metamorphic aureoles (Ferry et al., 2011, Lloyd et al., 2017). Vein-filling dolomite has δ18O values of ‰22.2–23.4‰ and δ13C values of ‰0.1–0.8‰, which are lower than the host rock and plot outside of the 'primary range' (Fig. 4). Annealed grains of primary dolomite in contact with the secondary minerals have a Δ47 value similar to the secondary dolomite and δ18O and δ13C values similar to the primary dolomite. Single- and clumped-isotope compositions of whole-rock sample NAX9 are mostly similar to the layer of annealed dolomite grains, suggesting this fabric makes up most of the rock fragments that were crushed and analyzed.

The primary dolomite apparent temperature of 290 °C is similar to those of other slowly cooled dolomites (Bonifacie et al., 2013), and likely reflects the solid-state isotopic reordering during exhumation-controlled cooling. Under geologically reasonable critical-shear-stress (>50 Mpa), dolomite deforms by dislocation glide at >700 °C (Davis et al., 2008). Thus, unlike calcite, the Δ47 value of dolomite will continue to reset to lower temperatures after dislocation glide had ceased under nearly any conceivable geological cooling rate. Therefore, dynamic recrystallization is not expected to affect the final observed Δ47 values of dolomites.

We interpret the composition of the vein fabric to reflect the temperature of the hydrothermal event and the presence of an isotopically light fluid (a calculation of the composition of fluid in equilibrium is given in section 3.6). Primary dolomite in contact with secondary dolomite also has high apparent temperatures (416±37°C), but preserves the single-isotope compositions of the host rock. This suggests a closed-system isotopic reordering occurred in response to the thermal pulse induced by the hypothesized hydrothermal event. A heating event is also supported by the grain annealing observed in the outmost millimeter of the host rock where it is in contact with the secondary dolomite (Fig. 7C).

Ultimately, Sample NAX9 re-enforces our suggestion that a hot hydrothermal event altered the Δ47 values of Naxos marbles, and that it did so both through water–rock reactions and through closed-system solid-state isotopic reordering in response to a thermal pulse. In this respect, this sample can be viewed as a mm-scale analog to a larger scale heat pulse delivered to the core through hydrothermal activity following the emplacement of the granodiorite pluton (in fact, these could be manifestations of the same event at different scales).

### 3.5. Deformation and re-precipitation at the rim of the core-complex

To study how retrograde deformation and re-precipitation processes are recorded in the single- and clumped-isotope compositions of carbonate that formed far from the influence of the plutonism and/or potential associated hydrothermal activity, we analyzed a calcite marble sample (NAX19) collected at the rim of the Naxos core-complex (Fig. 5B). Sample NAX19 is a mylonite consisting of few-millimeter-thick bands varying in color and grain size (Fig. 8A). Coarse grained bands have ‘core and mantle’ texture, with grain cores as large as 100–250 μm, which frequently contain twin lamella and display unduluse extinction, indicative of dynamic recrystallization (Fig. 8B). The finest carbonate mineral grains (<50 μm) are found in a 1–2 mm thick shear-band (zone 4 in Fig. 8A). Unlike the rest of the sample, the shear band contains both calcite and dolomite grains, and large (up to 200 μm) muscovite flakes, preferentially oriented parallel to the band (Fig. 8C). Sub-samples of the different bands yield a 0.401–0.566‰ Δ47 values range, which are negatively correlated with oxygen and carbon isotopic compositions (Fig. 8D).

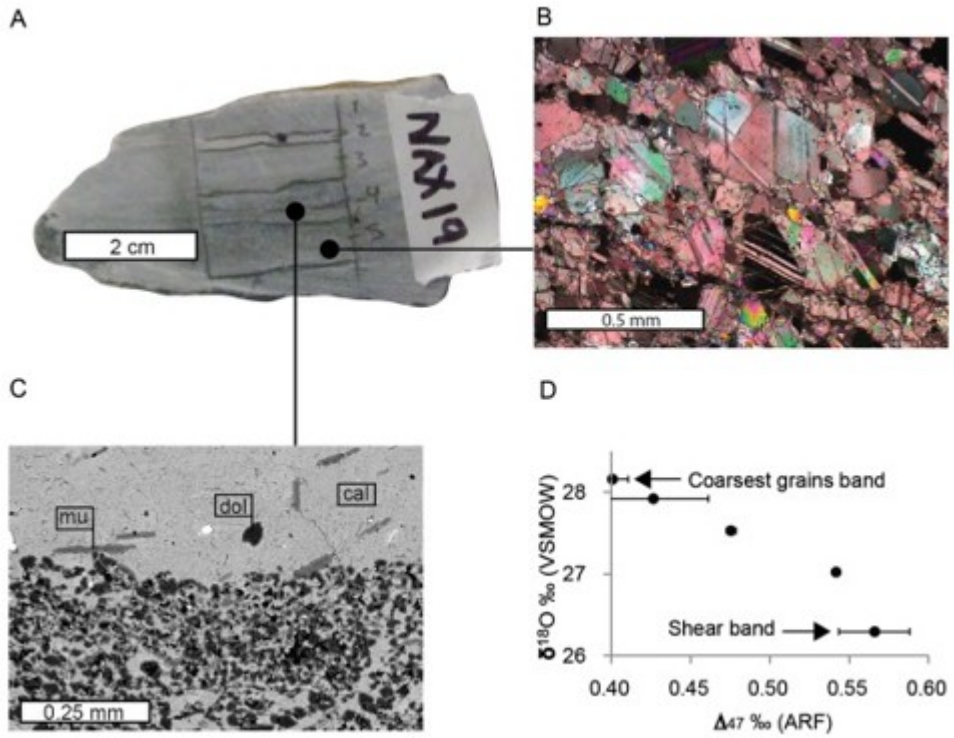


Fig. 8. Thin section and carbonate single- and clumped-isotope analyses results of sample NAX19. A) Photograph of sample NAX19, a calcite mylonite consisting of coarse and fine grained bands. Numbers refer to specific bands (marked by hand drawn lines) from which subsamples were drilled. B) Thin-section image (crossed nicols) of the coarsest-grained band. Unduluse extinction and 'core and mantle' structures are indicative of dynamic recrystallization (Shelley, 1993). Grain cores are typically twinned. C) Backscatter image of the contact between the coarsest- and shear-bands. 'cal' – calcite, 'dol' – dolomite, and 'mu' – muscovite. Muscovite flakes are oriented parallel the shear band. D) $\Delta_{47}$ values of sampled zones plotted against $\delta^{18}O$ composition; see text for details. Error bars are 1 S.E. for $\Delta_{47}$ values, and smaller than the symbol for $\delta^{18}O$.

We interpret the linear trend in Fig. 8D as a mixing line between two end-members with different single- and clumped-isotope compositions: One end-member, is likely the coarse-grain band (Fig. 8A).
Its δ18O and δ13C composition (28.2‰ and 1.8‰, respectively) lies within the 'primary range' (Fig. 4), and its Δ47 value (‰0.401±0.011‰ (1 S.E.)) corresponds to an apparent temperature of 205 °C (Fig. 8D). This value is indistinguishable from blocking temperatures of calcite marbles that cooled over geological timescales (1–1000 °C $Myr^{-1}$) (Bonifacie et al., 2011, Passey and Henkes, 2012, Stolper and Eiler, 2015). The other end-member, identified in the shear band (Fig. 8C), has lower δ18O and δ13C values (26.3‰ and ‰−1.7‰, respectively) that plot outside the 'primary range' (Fig. 4), and a higher Δ47 value (‰0.567±0.022‰ (1 S.E.)), corresponding to an apparent temperature of 70 °C (Fig. 8D). The whole-rock clumped- and single-isotope compositions of sample NAX19 are consistent with the suggested mixing between the above end-members.

The apparent temperature of 205 °C for the first end-member is similar to the dynamically recrystallized calcite fabrics of sample NAX2. We interpret

this temperature to reflect the minimum temperature of dynamic recrystallization. The second end-member is attributed to the precipitation of secondary carbonates (both calcite and dolomite) from an isotopically light fluid at ≤70 °C. Since the sampled shear-band may contain non-secondary minerals, we regard its δ18O and δ13C compositions as the maximum values for secondary minerals, and the apparent temperature as their maximum temperature of formation. This temperature is below the minimum temperature of dynamic recrystallization, which leads to the prediction that secondary minerals should not be preferentially oriented (Shelley, 1993). We tested this prediction using EBSD analyses of the calcite in the two end-member fabrics. In the coarsest grain band, calcite has a distinct crystal preferred orientation, consistent with the direction of the bands and the orientation of the muscovite flakes (Fig. 9A). In the fine grained shear band, calcite lacks crystal-preferred orientation (Fig. 9B), consistent with post deformational re-precipitation of carbonates. Higher proportions of re-precipitation, and the presence of dolomite in the shear-band, possibly resulted from their higher hydraulic conductivity and increased reactivity.

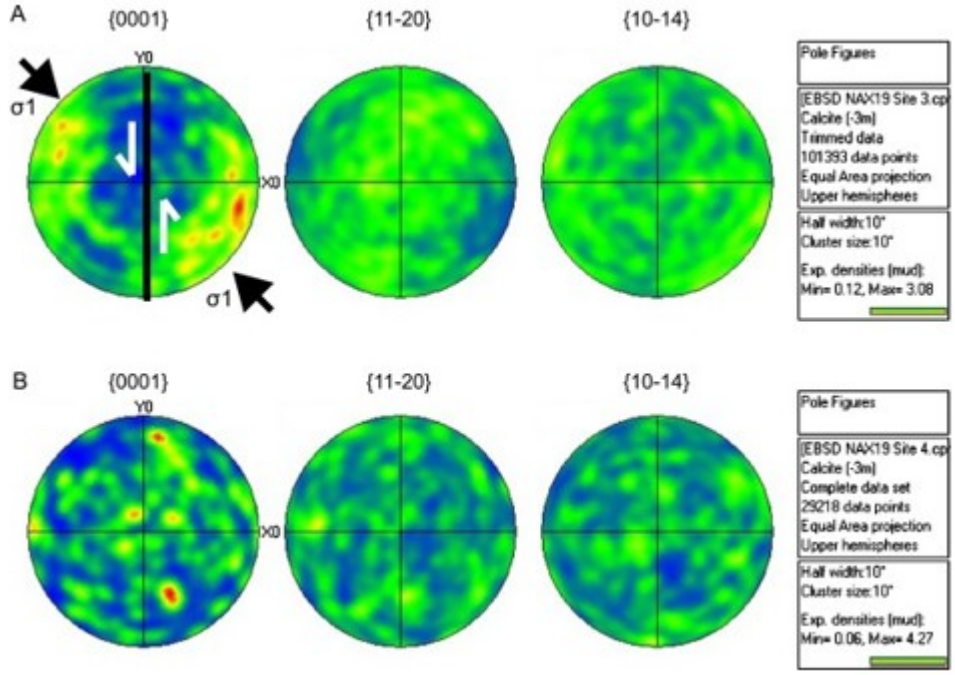


Fig. 9. Crystal preferred orientation of calcite in sample NAX19. EBSD pole figures are plotted using an equal-area projection of c axes {0001}, and of r {10–14}, and a {11–20} planes, on the upper-hemisphere. A) EBSD pole figure of the coarsest-grain band. Projection of the c axes {0001} shows a distinct pattern. In a simple shear, c-axes are expected to lie close to the main compression stress ($\sigma 1$), consistent with a left-lateral slip parallel to the shear bend (thick black vertical line). B) EBSD pole figure of calcite in the shear-band. No significant pattern emerges.

### 3.6. The characteristics and source of fluids in the exhuming core-complex

Magmatic, metamorphic, meteoric and marine sources have been proposed for the fluids that interacted with the metamorphic complex on Naxos (Baker et al., 1989, Baker and Matthews, 1995, Matthews et al., 2002, Siebenaller et

al., 2013). Here we use temperatures of formation of secondary minerals to calculate the isotopic composition of the parent fluids in equilibrium with those minerals and to evaluate their likely sources. We assume that all oxygen in the fluid was contained as H2O, and that all carbon was contained as $CO_2$ or HCO3− molecules. Using equilibrium isotope fractionation factors for calcite (Bottinga, 1968, O'Neil et al., 1969) and dolomite (Horita, 2014) corresponding to the apparent temperatures of secondary minerals, we calculate fluid composition in equilibrium with secondary dolomite (δ18O of 2.8‰ and δ13C of ‰−4.5‰) and with calcite (δ18O of 5.6‰ and δ13C of ‰−3.4‰) in sample NAX19 (Fig. 4). The calculation of fluid δ13C composition assumes HCO3− is the dominant dissolved carbon species at a temperature of 70 °C and a pH>7 (expected in a carbonate rock environment) (Benezeth et al., 2013), and therefore considers the fractionation between carbonate-minerals and HCO3− (Fig. 4, Mook et al., 1974).

Since the single-isotope compositions of sample NAX19 is regarded as the maximum value for the secondary minerals, and secondary calcite is isotopically heavier than dolomite, the single-isotope compositions of fluid in equilibrium with calcite defines the maximum possible values for the parental fluid (Fig. 4, gray rectangle ‘2’). This calculated range of δ18Ocomposition (‰≤5.6‰) is lower than most igneous and metamorphic waters (6–10 and 5–25‰, respectively), and overlaps with some marine pore-waters (−8 to 8‰), and meteoric- or unmodified sea-water (Taylor, 1974) (Fig. 4). Calculated δ13C values are similar though slightly lower than marine limestones (‰~0‰).

Similarly, we calculated the single isotope composition of the fluid in equilibrium with secondary dolomite from sample NAX9 to be 18.6‰ for δ18O and 4.1‰ for δ13C. At 380 °C dissolved inorganic carbon is dominated by $CO_2$ (Benezeth et al., 2013). Therefore we use the fractionation factor between carbonate mineral and $CO_2$ for this calculation. The calculated δ18O value is consistent with a metamorphic-water source (Fig. 4) and likely reflects the buffering of pore water by the carbonate rock. The calculated single isotope compositions of parental fluids of secondary minerals are largely consistent with the hydrothermal circulation of marine pore-water and, near the center of the core, with a metamorphic-water source.

## 4. Summary and conclusions

Calcite and dolomite marbles from Naxos, Greece, show large variations of clumped- and single-isotope values that reflect the combined influences of thermal history, deformation, and water- rock reactions, occurring in open- or closed-system conditions. Although complex, these processes leave distinctive, interpretable isotopic signatures in the fabrics found in marbles.

We find that dynamic recrystallization can reset the Δ47 values of calcites. This process is attributed to the efficient mobilization of carbonate ion-

groups during slip along crystallographic planes. Consequently, measured apparent temperatures of dynamically recrystallized calcites constrain the minimum temperature of dynamic recrystallization.

Secondary minerals that fill dissolution voids in marbles may capture both the temperature and the isotopic composition of their parental fluids. However, the effects of hydrothermal activity are not limited to secondary minerals, as the heat released by the hot fluids can alter the Δ47 value of the host rock through solid-state isotopic reordering.

The combination of our results with published thermochronometry data suggests that the center of Naxos' metamorphic core-complex cooled rapidly to below ~60 °C at ~12 Ma. The rate of this cooling event is attributed to the relaxation of a brief heat-pulse that occurred late in the exhumation history, possibly delivered by hydrothermal activity that followed the emplacement of a granodiorite pluton at that time. The heating event triggered dynamic recrystallization of calcite marbles along shear-bands and annealed deformed dolomite grains. The single-isotope compositions of the hydrothermal fluid is consistent with a marine pore fluid near the edges of the core-complex and with metamorphic water near its center.

Acknowledgments

The authors wish to thank Dov Avigad for his invitation to join HUJI field-trip to the Aegean Islands, and Avishai Abbo and Michal Ben-Israel for their assistance in the field. We thank Ken Farley for fruitful discussions and for enabling the U–Th/He measurements. We thank Nami Kitchen, Lindsey Hedges, and Chi Ma for helping with sample preparation and analyses. We thank three anonymous reviewers for their detailed and constructive comments. UR was supported by the O.K. Earl Scholarship during this study.

References

Altherr et al., 1979

R. Altherr, M. Schliestedt, M. Okrusch, E. Seidel, H. Kreuzer, W. Harre, H. Lenz , I. Wendt, G.A. Wagner**Geochronology of high-pressure rocks on Sifnos (Cyclades, Greece)**

Contrib. Mineral. Petrol., 70 (1979), pp. 245-255

Andriessen et al., 1979

P.A.M. Andriessen, N.A.I.M. Boelrijk, E.H. Hebeda, H.N.A. Priem, E.A.T. Verdur men, R.H. Verschure**Dating the events of metamorphism and granitic magmatism in the Alpine orogen of Naxos (Cyclades, Greece)**

Contrib. Mineral. Petrol., 69 (1979), pp. 215-225

Avigad, 1998

D. Avigad**High-pressure metamorphism and cooling on SE Naxos (Cyclades, Greece)**

Eur. J. Mineral., 10 (1998), pp. 1309-1319

Baker et al., 1989

J. Baker, M.J. Bickle, I.S. Buick, T.J.B. Holland, A. Matthews**Isotopic and petrological evidence for the infiltration of water-rich fluids during the Miocene M2 metamorphism on Naxos, Greece**

Geochim. Cosmochim. Acta, 53 (1989), pp. 2037-2050

Baker and Matthews, 1994

J. Baker, A. Matthews**Textural and isotopic development of marble assemblages during the Barrovian-style M2 metamorphic event, Naxos, Greece**

Contrib. Mineral. Petrol., 116 (1994), pp. 130-144

Baker and Matthews, 1995

J. Baker, A. Matthews**The stable isotopic evolution of a metamorphic complex, Naxos, Greece**

Contrib. Mineral. Petrol., 120 (1995), pp. 391-403

Benezeth et al., 2013

P. Benezeth, A. Stefansson, Q. Gautier, J. Schott**Mineral solubility and aqueous speciation under hydrothermal conditions to 300 °C – the carbonate system as an example**

Rev. Mineral. Geochem., 76 (2013), pp. 81-133

Bickle and Baker, 1990

M.J. Bickle, J. Baker**Advective diffusive transport of isotopic fronts – an example from Naxos, Greece**

Earth Planet. Sci. Lett., 97 (1990), pp. 78-93

Bonifacie et al., 2013

M. Bonifacie, D. Calmels, J.M. Eiler**Clumped isotope thermometry of marbles as an indicator of the closure temperatures of calcite and dolomite with respect to solid-state reordering of C–O bonds**

Mineral. Mag., 77 (2013), p. 735

Bonifacie et al., 2017

M. Bonifacie, D. Calmels, J.M. Eiler, J. Horita, C. Chaduteau, C. Vasconcelos, P. Agrinier, A. Katz, B.H. Passey, J.M. Ferry, J.-J. Bourrand**Calibration of the dolomite clumped isotope thermometer from 25 to 350 °C, and implications for a universal calibration for all (Ca, Mg, Fe)$CO_3$ carbonates**

Geochim. Cosmochim. Acta, 200 (2017), pp. 255-279

Bonifacie et al., 2011

M. Bonifacie, J.M. Ferry, J. Horita, C. Vasconcelos, B.H. Passey, J.M. Eiler**Calibration and applications of the dolomite clumped isotope thermometer to high temperatures**

Mineral. Mag., 75 (2011), p. 551

Bottinga, 1968

Y. Bottinga**Calculation of fractionation factors for carbon and oxygen isotopic exchange in the system calcite-carbon dioxide-water**

J. Phys. Chem., 72 (1968), pp. 800-808

Brichau et al., 2006

S. Brichau, U. Ring, R.A. Ketcham, A. Carter, D. Stockli, M. Brunel**Constraining the long-term evolution of the slip rate for a major extensional fault system in the central Aegean, Greece, using thermochronology**

Earth Planet. Sci. Lett., 241 (2006), pp. 293-306

Bristow et al., 2011

T.F. Bristow, M. Bonifacie, A. Derkowski, J.M. Eiler, J.P. Grotzinger**A hydrothermal origin for isotopically anomalous cap dolostone cements from South China**

Nature, 474 (2011), pp. 68-92

Burkhard, 1993

M. Burkhard**Calcite twins, their geometry, appearance and significance as stress–strain markers and indicators of tectonic regime – a review**

J. Struct. Geol., 15 (1993), pp. 351-368

Covey-Crump and Rutter, 1989

S.J. Covey-Crump, E.H. Rutter**Thermally-induced grain-growth of calcite marbles on Naxos Island, Greece**

Contrib. Mineral. Petrol., 101 (1989), pp. 69-86

Davis et al., 2008

N.E. Davis, A.K. Kronenberg, J. Newman**Plasticity and diffusion creep of dolomite**

Tectonophysics, 456 (2008), pp. 127-146

DeBresser and Spiers, 1997

J.H.P. DeBresser, C.J. Spiers**Strength characteristics of the r, f, and c slip systems in calcite**

Tectonophysics, 272 (1997), pp. 1-23

Defliese et al., 2015

W.F. Defliese, M.T. Hren, K.C. Lohmann**Compositional and temperature effects of phosphoric acid fractionation on** Δ47 **analysis and implications for discrepant calibrations**

Chem. Geol., 396 (2015), pp. 51-60

Dennis et al., 2011

K.J. Dennis, H.P. Affek, B.H. Passey, D.P. Schrag, J.M. Eiler**Defining an absolute reference frame for 'clumped' isotope studies of $CO_2$**

Geochim. Cosmochim. Acta, 75 (2011), pp. 7117-7131

Eiler, 2011

J.M. Eiler**Paleoclimate reconstruction using carbonate clumped isotope thermometry**

Quat. Sci. Rev., 30 (2011), pp. 3575-3588

Essene, 1989

E.J. Essene**The current status of thermobarometry in metamorphic rocks**

J.S. Daly, R.A. Cliff, B.W.D. Yardley (Eds.), Evolution of Metamorphic Belts, Spec. Publ. - Geol. Soc. Lond. (1989), pp. 1-44

Farley, 2002

K.A. Farley**(U–Th)/He dating: techniques, calibrations, and applications**

Noble Gases in Geochemistry and Cosmochemistry, vol. 47 (2002), pp. 819-844

Ferry et al., 2011

J.M. Ferry, B.H. Passey, C. Vasconcelos, J.M. Eiler**Formation of dolomite at 40–80 °C in the Latemar carbonate buildup, Dolomites, Italy, from clumped isotope thermometry**

Geology, 39 (2011), pp. 571-574

Flowers et al., 2008

R.M. Flowers, B.P. Wernicke, K.A. Farley**Unroofing, incision, and uplift history of the southwestern Colorado Plateau from apatite (U–Th)/He thermochronometry**

Geol. Soc. Am. Bull., 120 (2008), pp. 571-587

Ganor et al., 1994

J. Ganor, A. Matthews, M. Schliestedt**Post-metamorphic low Delta-C-13 calcite in the Cycladic complex (Greece) and their implications for**

**modeling fluid infiltration processes using carbon-isotope compositions**

Eur. J. Mineral., 6 (1994), pp. 365-379

Ghosh et al., 2006

P. Ghosh, J. Adkins, H. Affek, B. Balta, W.F. Guo, E.A. Schauble, D. Schrag, J.M. Eiler**$^{13}C$–$^{18}O$ bonds in carbonate minerals: a new kind of paleothermometer**

Geochim. Cosmochim. Acta, 70 (2006), pp. 1439-1456

Hejl et al., 2003

E.H.R. Hejl, N. Soulakellis, P. Van Den Haute, H. Weingartner**Young Neogene tectonics and relief development on the Aegean islands of Naxos, Paros and Los (Cyclades, Greece)**

Mitt. Österr. Geol. Ges., 93 (2003), pp. 105-127

Henkes et al., 2014

G.A. Henkes, B.H. Passey, E.L. Grossman, B.J. Shenton, A. Perez-Huerta, T.E. Yancey**Temperature limits for preservation of primary calcite clumped isotope paleotemperatures**

Geochim. Cosmochim. Acta, 139 (2014), pp. 362-382

Horita, 2014

J. Horita**Oxygen and carbon isotope fractionation in the system dolomite-water–$CO_2$ to elevated temperatures**

Geochim. Cosmochim. Acta, 129 (2014), pp. 111-124

Huntington et al., 2009

K.W. Huntington, J.M. Eiler, H.P. Affek, W. Guo, M. Bonifacie, L.Y. Yeung, N. Thiagarajan, B. Passey, A. Tripati, M. Daeron, R. Came**Methods and limitations of 'clumped' $CO_2$ isotope ($\Delta 47$) analysis by gas-source isotope ratio mass spectrometry**

J. Mass Spectrom., 44 (2009), pp. 1318-1329

Jansen and Schuiling, 1976

J.B.H. Jansen, R.D. Schuiling**Metamorphism on Naxos – petrology and geothermal gradients**

Am. J. Sci., 276 (1976), pp. 1225-1253

John and Howard, 1995

B.E. John, K.A. Howard**Rapid extension recorded by cooling-age patterns and brittle deformation, Naxos, Greece**

J. Geophys. Res., Solid Earth, 100 (1995), pp. 9969-9979

Karato, 2008

S.I. Karato**Deformation of Earth Materials: An Introduction to the Rheology of Solid Earth**

Cambridge University Press, Cambridge, New York (2008)

Lloyd et al., 2015

M.K. Lloyd, J.M. Eiler, P.I. Nabelek**The clumped isotope geochemistry of dolomite and calcite in contact metamorphic environments**

Mineral. Mag., 1908 (2015)

Lloyd et al., 2017

M.K. Lloyd, J.M. Eiler, P.I. Nabelek**Clumped isotope thermometry of calcite and dolomite in a contact metamorphic environment**

Geochim. Cosmochim. Acta, 197 (2017), pp. 323-344

Matthews et al., 2002

A. Matthews, J. Baker, D.P. Mattey**High-temperature metamorphism in marbles as a consequence of volatile release from crystallizing anatectic melts, Naxos, Greece**

Eur. J. Mineral., 14 (2002), pp. 37-47

Mook et al., 1974

W.G. Mook, J.C. Bommerso, W.H. Staverma**Carbon isotope fractionation between dissolved bicarbonate and gaseous carbon-dioxide**

Earth Planet. Sci. Lett., 22 (1974), pp. 169-176

O'Neil et al., 1969

J.R. O'Neil, R.N. Clayton, T.K. Mayeda**Oxygen isotope fractionation in divalent metal carbonates**

J. Chem. Phys., 51 (1969), p. 5547

Passey and Henkes, 2012

B.H. Passey, G.A. Henkes**Carbonate clumped isotope bond reordering and geospeedometry**

Earth Planet. Sci. Lett., 351–352 (2012), pp. 223-236

Passey et al., 2010

B.H. Passey, N.E. Levin, T.E. Cerling, F.H. Brown, J.M. Eiler**High-temperature environments of human evolution in East Africa based on bond ordering in paleosol carbonates**

Proc. Natl. Acad. Sci. USA, 107 (2010), pp. 11245-11249

Reiners et al., 2005

P.W. Reiners, T.A. Ehlers, P.K. Zeitler**Past, present, and future of thermochronology**

Rev. Mineral. Geochem., 58 (2005), pp. 1-18

Ring et al., 2010

U. Ring, J. Glodny, T. Will, S. Thomson**The hellenic subduction system: high-pressure metamorphism, exhumation, normal faulting, and large-scale extension**

Annu. Rev. Earth Planet. Sci., 38 (2010), pp. 45-76

Rutter and Brodie, 1995

E.H. Rutter, K.H. Brodie**Mechanistic interactions between deformation and metamorphism**

Geol. J., 30 (1995), pp. 227-240

Rye et al., 1976

R.O. Rye, R.D. Schuiling, D.M. Rye, J.B.H. Jansen**Carbon, hydrogen, and oxygen isotope studies of regional metamorphic complex at Naxos, Greece**

Geochim. Cosmochim. Acta, 40 (1976), pp. 1031-1049

Schliestedt et al., 1987

M. Schliestedt, R. Altherr, A. Matthews**Evolution of the cycladic crystalline complex: petrology, isotope geochemistry and geochronolgy**

H.C. Helgeson (Ed.), Chemical Transport in Metasomatic Processes, D. Reidel Publishing Company(1987), pp. 389-428

Seward et al., 2009

D. Seward, O. Vanderhaeghe, L. Siebenaller, S. Thomson, C. Hibsch, A. Zingg, P. Holzner, U. Ring, S. Duchene**Cenozoic tectonic evolution of Naxos Island through a multi-faceted approach of fission-track analysis**

Geol. Soc. Spec. Publ., 321 (2009), pp. 179-196

Shelley, 1993

D. Shelley**Igneous and Metamorphic Rocks Under the Microscope: Classification, Textures, Microstructures, and Mineral Preferred-Orientations**

Chapman & Hall, London, New York (1993)

Siebenaller et al., 2013

L. Siebenaller, M.C. Boiron, O. Vanderhaeghe, C. Hibsch, M.W. Jessell, A.S. An dre-Mayer, C. France-Lanord, A. Photiades**Fluid record of rock**

**exhumation across the brittle-ductile transition during formation of a metamorphic core complex (Naxos Island, Cyclades, Greece)**

J. Metamorph. Geol., 31 (2013), pp. 313-338

Siman-Tov et al., 2016

S. Siman-Tov, P.H. Affek, A. Matthews, E. Aharonov, Z. Reches**Shear heating and clumped isotope reordering in carbonate faults**

Earth Planet. Sci. Lett., 445 (2016), pp. 136-145

Stolper and Eiler, 2015

D.A. Stolper, J.M. Eiler**The kinetics of solid-state isotope-exchange reactions for clumped-isotopes: a study of inorganic calcites and apatites from natural and experimental samples**

Am. J. Sci., 315 (2015), pp. 363-411

Swanson et al., 2012

E.M. Swanson, B.P. Wernicke, J.M. Eiler, S. Losh**Temperatures and fluids on faults based on carbonate clumped-isotope thermometry**

Am. J. Sci., 312 (2012), pp. 1-21

Taylor, 1974

H.P. Taylor**The application of oxygen and hydrogen isotope studies to problems of hydrothermal alteration and ore deposition**

Econ. Geol., 69 (1974), pp. 843-883

Urai et al., 1990

J.L. Urai, R.D. Schuiling, J.B.H. Jansen**Alpine deformation on Naxos (Greece)**

Deformation Mechanisms, Rheology and Tectonics, vol. 54 (1990), pp. 509-522

Wang et al., 2004

Z.G. Wang, E.A. Schauble, J.M. Eiler**Equilibrium thermodynamics of multiply substituted isotopologues of molecular gases**

Geochim. Cosmochim. Acta, 68 (2004), pp. 4779-4797

Whittington et al., 2009

A.G. Whittington, A.M. Hofmeister, P.I. Nabelek**Temperature-dependent thermal diffusivity of the Earth's crust and implications for magmatism**

Nature, 458 (2009), pp. 319-321

Wijbrans and Mcdougall, 1988

J.R. Wijbrans, I. Mcdougall**Metamorphic evolution of the attic cycladic metamorphic belt on Naxos (Cyclades, Greece) utilizing Ar-40/Ar-39 age spectrum measurements**

J. Metamorph. Geol., 6 (1988), pp. 571-594